CONF-
780902--19
LBL-8904

Presented at the American Chemical Society Meeting, Miami, Florida, September 10-15, 1978

STUDIES OF ACTINIDE SORPTION ON SELECTED GEOLOGIC MATERIALS

R. J. Silva, L. V. Benson, and J. A. Apps

September 1978

Prepared for the U. S. Department of Energy
under Contract W-7405-ENG-48

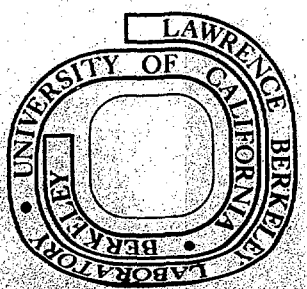

Studies of Actinide Sorption on Selected Geologic Materials

R. J. Silva, L. V. Benson, and J. A. Apps

Earth Sciences Division
Lawrence Berkeley Laboratory
Berkeley, California 94720

Introduction

The long term objective of this program is to establish a basis for the prediction of radionuclide sorption in geologic environments of the type anticipated for terminal radioactive waste storage. In order to begin to identify parameters which should be incorporated in a predictive sorption model, a study of the interaction of U, Np, Pu, Am, and Cm with basalt, shale and granite was initiated. The following discussion covers the experimental results to date. The mineral makeup of the rocks and the composition of the solutions were determined so that as the dependence of nuclide adsorption on these parameters becomes better known, the results of these experiments may be understood in greater detail.

The sorption/desorption processes were studied by a batch type technique. Aqueous solutions were prepared by mixing rock powders with distilled-deionized water. For the sorption experiments, portions of these aqueous solutions were loaded with tracer quantities of a single radioactive nuclide and contacted with wafers of a given rock type. For the desorption experiments, wafers from the sorption experiments were contacted with the remaining portions of the aqueous solutions.

The progress of the contact experiments was monitored by gamma-ray counting of solutions. Actinide tracer concentrations on the wafers and in the solutions were measured at the end of the contact period by alpha and gamma-ray counting. These data were used to calculate sorption coefficients. Autoradiography of the wafers is being performed to gather information on sorption specificity.

Selection of Rock Samples and Tracers

Radionuclides. Isotope selection was based primarily on three experimental requirements: (1) both alpha and gamma emitters present for counting purposes; (2) alpha emitter present for autoradiography; (3) approximately equal

molar concentration of the elements at the start of sorption experiments. Table I shows the isotopic compositions of the tracer solutions and the photons used for gamma counting of samples. In the case of U, Np, and Am, the single isotopes ^{233}U, ^{237}Np, and ^{243}Am were used for both alpha and gamma counting. In the case of Pu, the isotope ^{237}Pu was used for gamma counting, while ^{242}Pu was used for alpha counting and for adjusting the molar concentration. The ^{243}Cm was used for both alpha and gamma counting and ^{248}Cm to adjust the molar concentration. Small amounts of other isotopes made during the production processes were also present in most of the samples.

Rock Samples. Three rock types were selected as substrates: basalt from the Umtanum unit in the Pasco Basin in Washington state, quartz monzonite from the Climax Stock of the Nevada Test Site, and shale (metashale) from the Eleana Formation of the Nevada Test Site. Since both the basalt and the quartz monzonite exhibited different kinds and amounts of alteration within the same rock type, two samples from each rock type were used in the experiments. However, there was insufficient material to study the interaction of the more altered of these rock types with all five actinides, therefore, only the interaction with Pu was studied.

Sample Characterization

Physical and chemical analyses of the samples were made in order to interpret the results of the sorption experiments and to provide basic data for the calculation of mass transfer which occurred in the rock dissolution experiment. Cores, 3.2 cm in diameter, were taken from each of the rock samples and sectioned in tap water for subsequent analyses (Figure 1).

Petrographic Studies. Polished thin sections were examined by optical methods to determine original mineralogy and alteration phases. The sections were taken and oriented in such a manner to allow comparison of the microscopic mineralogy with the results of the autoradiography experiments. The shale was too fine-grained to be characterized in detail.

Both basalt samples (DC3-3600 and DH5-2831) are composed primarily of glass (40-50 percent) and plagioclase feldspar (35-40 percent). They contain in addition minor amounts of clinopyroxene (3-5 percent) orthopyroxene (1 percent), and opaques (1-2 percent). The relatively unaltered basalt (DC3-3610) possesses several intersecting fractures filled with clay. There are dark gray alteration zones adjacent to certain fractures where a smectitic clay has replaced

glass and feldspars. Both plagioclase and clinopyroxene have been replaced by secondary minerals (clay, chlorite) along crystal faces and cleavage planes. In the vesicular basalt, (DH5-2831) approximately 40-50 percent of the vesicles remain unfilled; the rest are usually filled with cristobalite.

The quartz monzonite samples (U15E-7 and U15E-7a) were originally composed of 70-80 percent feldspar, 10-15 percent biotite, 3-8 percent quartz, and 2-8 percent opaques. Both samples have been hydrothermally altered; U15E-7a being the more altered. The original feldspars in both samples have been sericitized and/or altered to clinozoisite. Secondary calcite also occurs in both samples. Pyrite is an abundant secondary mineral and minor amounts of both epidote and chlorite replace biotite and fill fractures.

Scanning electron microscopy (SEM). SEM studies of the shale and the quartz monzonite samples were not feasible since the morphology of secondary minerals could not be explicitly identified by this technique. Energy dispersive analysis by x-rays (EDAX) of the clay in fractures of the DC3-3600 basalt sample indicated the presence of Fe, Mg, Ca, K, Al, and Si which suggests that the clay is an Fe- and Mg-rich smectite (nontronite). SEM and EDAX studies of DH5-2831, the amygdalic basalt, indicated the presence of a pure silica phase coated by small clay (smectite) particles. Other vesicles "floored" with pure silica were covered with a relatively thick coating of the smectite. In addition, one vesicle was filled with gypsum fibers intermixed with an irregularly-shaped aluminosilicate containing Na, K, and Ca.

X-ray diffraction studies. The highly-altered quartz monzonite (U15E-7a) was examined with x-ray diffraction techniques. Four regions, distinguishable in hand specimens by their color, (metallic, pink, dark-gray, and yellow-gray) were sampled and analyzed. The results (Table II) support the petrographic observations and indicate that the original calcic feldspars have been altered to potassium-bearing phases (potassium feldspar or sericite) or to other secondary calcium-bearing minerals (calcite and clinozoisite).

Bulk chemical analysis of the solids. The three rock types were chemically analyzed by neutron activation (NAA) and x-ray fluorescence (XRF). The resulting data (not included in this report) were used for depth-of-leaching calculations given below. With the measurement of volatile components in the basalt and shale, the total measured abundances in all three samples was close to 100 percent.

Characterization of physical properties. A variety of physical properties were measured including density, specific

surface area, permeability, and pore characteristics (Table III). Pore volume was determined by the mercury injection method on a Micromeritics Model 900/910 Porosimeter and also by measuring the volume of gas which flowed into the sample under ambient conditions. Specific surface area was determined both on a Model 2100 Orr Analyzer and on a QUANTASORB Surface Area Analyzer by the standard multipoint BET technique using krypton and nitrogen adsorption. Permeability was measured by introducing a gas pressure pulse and monitoring pressure decay (transient method).

Certain of the physical data (Table III) appear to be less than satisfactory. In general, agreement between the two types of porosity measurements is not good and the values for DC3-3600, UE15-7 and UE15-7a appear excessively large. The densities of the quartz monzonite appear unusually low, i.e., values in the range 2.6 to 2.7 were expected (1).

Purification and Characterization of Actinide Tracers

Before the tracer solutions were used, it was necessary to insure elemental purity and freedom from other contaminants. In addition, one oxidation state was selected for each element as the starting point for the experiments. The 6+ oxidation state for U, 5+ for Np, 4+ for Pu, and 3+ for both Am and Cm were used. These selections were accomplished through the use of cation-exchange chromatography. A given radionuclide was first sorbed on the top of a cation-exchange resin column from a dilute hydrochloric acid solution and, after washing, selectively eluted with a hydrochloric acid solution appropriate for the given oxidation state. The column characteristics and chemical form of each radionuclide are shown in Table IV. After column elution, all tracers were made up to nearly equal molar concentration in 2M HCl.

The Dissolution Experiment

It was necessary to prepare an aqueous electrolyte solution for the sorption study. To simulate sorption processes which occur in natural systems, the electrolyte solution should fulfill two criteria:

(1) The composition of the solution should closely approximate the natural aqueous phase so that the effects of ion pairing and complexation are accounted for.

(2) The solution should be in equilibrium with the solid's surface with respect to all chemical processes excepting sorption/desorption. If the solid dissolves, the surface energy distribution and the composition of the aqueous phase will constantly change. If precipitation occurs, the surface of the solid may become coated with pre-

cipitate, thus altering the character of the sorptive substrate.

In order to produce an aqueous solution which fulfills these criteria, 120 g each of basalt, quartz monzonite, and shale were ground to powders less than 37 m in diameter. Each of the samples was placed in two liters of distilled-deionized water which had been pre-equilibrated with an atmosphere containing 10 percent CO_2, 90 percent Ar, and 10 ppm O_2. The experiment was carried out in an inert atmosphere box at room temperature (26 ± 2°C). Samples of the fluid (10 ml) were extracted at various times over a 35-day period and filtered (0.05μm). Analyses for Na, K, Mg, Ca, Fe, Al, SiO_2 (aq), Eh, and pH were made on each sample. The experiment was terminated at the end of 846 hours and analyses for HCO_3, SO_4, and Cl were made on each of the fluids.

Reaction rates. The molar concentrations of Na, K, Ca, Mg, and SiO_2, as well as pH, plotted as a function of elapsed time are shown in Figures 2 to 7. With some variation, a similar pattern is displayed by all three rock types: an initial steep portion followed by an approximately linear region with small positive slope. Exceptions to this can be seen in Figure 2 where Na in the shale solution has a slightly negative slope, in Figure 3 where K in the shale solution has essentially zero slope, and in Figure 6 where the overall dissolution pattern of SiO_2 appears roughly parabolic.

The release of cations is interpreted to have resulted chiefly from two processes: an initial release caused by rapid exchange of surface cations for hydrogen followed by a slow release due to structural attack and disintegration of the aluminosilicate lattice. Other processes which could complicate the form of the dissolution curves are: adsorption of cations released by structural breakdown, ion exchange on interlayer sites of cations released by structural breakdown and surface exchange (shale only), precipitation of amorphous or crystalline material, and dissolution rate differences among the various crystalline phases.

Structural breakdown. Calculations of the depth of leaching/ dissolution were made using the following assumptions:

(1) The rock powder was assumed to have a homogeneous distribution of elements;
(2) All atomic sites were equivalent in size and had a cubic geometry;
(3) The most mobile cation (the cation which showed the largest concentration increase in the solution relative to its concentration in the solid) did not participate in precipitation or adsorption processes.

These calculations were made for the basalt and quartz

monzonite experiments only, since the shale experiment may have involved other complicating processes such as ion exhange between the aqueous phase and interlayer sites. Both the depth of leaching/dissolution that occurred during the entire experiment and the rate of leaching during the approximately linear portion of the experiment were determined. The results of these and other calculations are summarized in Table V. The data indicate that several atomic layers have been either totally stripped or have experienced diffusional processes (leaching) during the course of the experiment. The rate of release of cations during the linear region of the experiment was smaller than the initial release rate; however, the linear rate is still sufficient to have affected the solids to a depth of 0.4 (basalt) to 1.8 (quartz monzonite) atomic layers during the subsequent adsorption experiment which ran approximately six weeks (1006 hr). These calculations serve to point out the difficulties in eliminating interference effects during a long-term sorption experiment.

Final composition of the aqueous phase. The final compositions of the waters resulting from the three dissolution experiments have been summarized and listed together with compositions of waters from natural systems (Table VI). The experimental and natural basalt waters have very similar compositions. However, the experimental quartz monzonite water has a higher than natural K content while the shale water has higher than natural K and Na contents. The HCO_3 content of each of the experimental waters is higher than the content of its natural counterpart while the oposite is true for SO_4.

The differences in cation compositions are probably due to the fact that phases containing these ions (illite, smectite, etc.) have sufficient time to form in natural systems but did not form in the experimental system. The high HCO_3 content of the experimental system is due to contact with an infinite reservoir of CO_2 having a partial pressure of 0.1 atmosphere.

Rock/Tracer Contact Experiments

Procedure. The rock wafers were gently cleaned three successive times with methanol in an ultrasonic bath, dried and placed in the inert atmosphere box. Two wafers of each rock type were inserted horizontally in stainless steel holders and placed in linear polyethylene containers holding 150 ml of the appropriate prepared water. The wafers were allowed to equilibrate with the water for three days and then 5 λ of tracer solution was added. The resultant solutions contained $\sim 5 \times 10^{-8}$ M of each element. The pH of each solution was measured before and after the addition of the tracer and did not change sign-

ificantly. A blank solution not containing wafers was prepared in a similar manner for each of the five actinides by mixing 50 ml of each of the three water types. The containers were sealed, removed from the inert atmosphere box, and gently agitated with an Eberbach variable-speed shaker for six weeks.

The concentrations of tracers in solutions were determined periodically. The polyethylene containers were constructed in such a way that, when inverted, 50 ml of solution passed from the wafer compartment into a second compartment. The second compartment of the container was inserted through a hole in a lead shield which housed a 3.5 cm diameter by 1.2 cm deep high-purity Ge gamma-ray detector. The other compartment containing the solution and wafers was shielded from the detector by the lead housing.

At the end of the six weeks, the containers were returned to the inert atmosphere box and the wafers removed. One wafer was immediately placed in a new container with 50 ml of aqueous solution for the desorption study. The other wafer was rinsed lightly, allowed to dry and counted.

Aliquots of the solutions (50 ml) were placed in polyethylene bottles for gamma-ray counting and 0.5 ml samples were evaporated on platinum plates for alpha counting In addition, 10 ml of each of the solutions were passed through 0.05 μm Nucleopore filters. Aliquots (0.5 ml) of the last 2 ml passing the through filters were evaporated on platinum plates for alpha counting. Both alpha and gamma count rates on the wafers were measured.

Results and Discussion. Changes in concentrations of the actinides in solution in the blank containers are shown in Figure 9. A large fraction of the Pu, Am and Cm was removed from solution while only a small amount of the U and none of the Np was lost from solution. Since the starting concentration of Pu exceeds the solubility for the hydroxide (or hydrated oxide), the Pu probably precipitated as colloidal-size particles (2); the behavior of Am and Cm cannot be explained by a similar mechanism. However, there is recent experimental evidence that indicates the solubility products for Am and Cm carbonates may be of the order 10^{-41} (3). If this is the case, there was sufficient carbonate ion concentration in the solutions to cause precipitation of these compounds.

Figures 10, 11 and 12 show the results of the contact experiments for the basalt, shale and quartz monzonite samples. The rate of adsorption was rapid during the first two weeks and changed slowly thereafter. In these experiments Pu, Am and Cm exhibited behavior similar to the results obtained in the blank experiments. Uranium showed moderate adsorption ($\sim$ 50 percent) on the basalt but only slight adsorption (10-20 percent) on the shale and quartz monzonite wafers. Neptunium showed strong adsorption

(70-80 percent) on the shale and slight adsorption ($\sim$10 percent) on the basalt and quartz monzonite.

The calculated adsorption coefficients (K) are presented in Table VII. K (alpha) refers to results from alpha counting the wafers and solutions, while K (gamma) refers to results from gamma counting. K (filter) refers to results from the alpha counting of wafers and filtered solutions.

Measurement precision of the K values is $\pm$ 5-10 percent for K (alpha) and K (filter). Precision of the K (gamma) measurements are $\pm$ 5-10 percent for Am and Cm; $\pm$ 20 percent for Pu; and $\pm$30-35 percent for Np and U. These values represent only errors associated with the counting.

Except for Np, alpha counting showed that wafer surfaces facing upward consistently had higher counting rates than surfaces facing downward. The up/down ratios are also presented in Table VII. This behavior suggests that a process such as settling may be involved.

Comparisons of K (alpha) and K (gamma) show good agreement for each given rock type and element except for the shale samples. With the exception of Pu, K (gamma) values for the shale samples were considerably larger than K (alpha) values. Since alpha counting detects only material on the surface while gamma counting detects both surface and bulk-adsorbed material, adsorption on the basalt and quartz monzonite samples represents a surface process while the shale samples exhibit a diffusional effect in addition to surface sorption. Differential migration of the actinides into the samples was not expected since the measured permeabilities and porosities for the three rock types were nearly equivalent. However, as was noted above, the permeability and porosity data may be substantially in error.

Finally, a comparison of K (alpha) and K (filter) for each rock type and element show that, while the values for U and Np agree quite well, the values differ substantially for Pu, Am and Cm. Apparently, there were still considerable amounts of filterable or adsorbable species left in solution after the six week contact time.

The observed differences between the elements could presumably be attributed to differences in sorption properties of the chemical species present. Unfortunately, with the possible exception of Np, the lack of a complete set of thermodynamic data precludes a quantitative prediction of the concentrations of the various possible species in solution or of the conditions for the formation of solid phases. However, our data suggest that precipitation or colloid formation were the major reactions of Pu, Am and Cm in our solutions and, perhaps, a minor reaction of U.

The data obtained from the filtered solutions can be used to estimate an upper limit to the concentrations of soluble U, Pu, Am and Cm under the conditions of our experiments. These concentrations were approximately

$4x10^{-8}$M for U, $2x10^{-10}$M for Pu, and $2x10^{-11}$M for Am and Cm. Estimates of the concentrations of possible chemical species in solution for the four actinides were made using measured or estimated solubility, complexation and hydrolysis constants (4-8), and the measured OH^-, CO_3^{2-}, SO_4^{2-}, and Cl^- concentrations given in Table VI. The results showed that hydroxide and carbonate are the ligands that need to be considered; chloride and sulfate concentrations are sufficiently low that their effects may be neglected. The hydroxide and carbonate concentrations in our solutions were about $4x10^{-8}$M and $1x10^{-6}$M, respectively.

Solubility product constants of $10^{-11.73}$ and $10^{-22.4}$ have been reported (8) for uranyl carbonte and hydroxide, respectively. The hydroxide was calculated to be the stable solid phase under the conditions of our experiments. For the uranium concentrations used in our experiments, the dominant hydrolysis product was most likely $UO_2(OH)_2^0$; K $[UO_2^{2+} + 2OH^- = UO_2(OH)_2^0] = 10^{15.98}$ (8), saturated solution concentration = 10^{-7}M. The dominant carbonate complex was estimated as $UO_2CO_3^0$; K $[UO_2^{2+} + CO_3^{2-} = UO_2CO_3^0] = 10^{10.3}$ (8), saturation concentration = $5x10^{-4}$M. Since the starting concentration of U was $5x10^{-8}$M, precipitation was not expected to occur. Therefore, the reasons for the behavior of U in our experiments is not understood.

The hydroxide was expected to be the stable solid phase for Pu^{4+} under the conditions of our experiments. Reported and estimated solubility product constants range from 10^{-52} (7) to 10^{-62} (6). The major hydrolysis product for Pu^{4+} was estimated to be $Pu(OH)_4^0$; K $[Pu^{4+} + 4OH^- = Pu(OH)_4^0] = 10^{46.5}$ (6), saturation concentration range = 10^{-7}M to 10^{-16}M. Using this hydrolysis constant, an apparent solubility product quotient of 10^{-56} was calculated from our data. Unfortunately, reliable information does not exist for estimating the effects of carbonate complexing on the system. In addition, it has been suggested that PuO_2^+ is the major soluble species in equilibrium with the hydroxide precipitate under conditions similar to our experiments (9). Since neither of these effects were included, the calculated solubility quotient could be in error, i.e., too large.

In general, the chemical behavior of Am and Cm in solution are quite similar and similar to that of the trivalent lanthanides. The americium hydroxide and carbonate solubility product constants were estimated as $10^{-23.3}$ (6) and 10^{-33} (10), respectively, from published values on lanthanide compounds. The values for Cm would be expected to be nearly the same. The carbonate was calculated to be the stable solid phase. Because of the lack of experimental data on the hydrolysis and carbonate complexation constants, it is not possible to calculate the concentrations of the major species in our solutions. However, $Am(OH)^{2+}$ has been estimated (11) as the dominant hydrolysis product; K

$[Am^{3+} + OH^- = Am(OH)^{2+}] = 10^{8.08}$ (4). A saturation concentration of 10^{-7}M was calculated for this species in equilibrium with the solid carbonate. Since the starting concentration of Am was 5×10^{-8}M, precipitation was not anticipated. However, as mentioned previously, the assumed carbonate solubility may be high by eight orders of magnitude. From our data, solubility product quotients for the possible compounds, $Am_2(CO_3)_3$ and $AmOHCO_3$ were estimated as 10^{-41} and 10^{-25}, respectively. The values for Cm should be similar.

Rock/Tracer Desorption Experiments

Procedures. One of the rock wafers from each of the containers used in the adsorption experiments was placed in a new polyethylene bottle containing 50 ml of the appropriate aqueous solution. The containers were removed from the inert atmosphere box and gently agitated for six weeks. Tracer concentrations in the solution were measured periodically as described previously. At the end of six weeks, the experiments were terminated, the wafers removed from the containers, and the tracer concentrations of the components of the system determined in the same manner as in the adsorption experiments.

Results and Discussion. The data obtained from the gamma-ray spectra taken during the course of the desorption experiments were not useful for monitoring the rates of desorption. For the samples containing U and Np, only a small amount of activity appeared in solution and therefore the counting errors precluded a meaningful analysis. Though the counting errors for samples containing Pu, Am and Cm were small, large fluctuations in the measured values again made detailed analysis fruitless. However, there were some general trends that should be mentioned: most of the material that appeared in solution did so in 2 to 3 days; in general, the basalt and quartz monzonite wafers desorbed 3 to 5 times more tracer than the shale wafers; and the Pu, Am, and Cm values fluctuated a factor of 2 to 3 about the mean.

The distribution coefficients calculated from the alpha counting data are given in Table VIII. The gamma counting of the solutions is still in progress. The symbols are the same as used previously. For K (alpha), the counting precision is $\pm$ 10 percent for the U, Am and Cm samples and $\pm$ 20-30 percent for the Np and Pu samples. For K (filter), the counting precision is $\pm$ 10 percent for U, $\pm$ 10-20 percent for Np, Am and Cm and $\pm$30-40 percent for the Pu samples.

The up/down effect was also apparent in the data of the desorption experiment (Table VIII). However, only desorption data for shale differ significantly from the sorption data,

i.e., the up/down ratios are closer to unity in the desorption experiments. A comparison of K (alpha) and K (filter) show substantial differerences for Am, Cm, and Pu (basalt) samples.

Autoradiography of Rock Wafers

Procedure. At the completion of the sorption and desorption experiments, the rock wafers were placed in contact with Kodak AR.10 nuclear emulsion films to obtain alpha particle induced autoradiographs. Due to the low concentrations of tracers on many of the wafers, rather lengthy exposure times (up to three months) are needed to obtain autoradiographs that can be readily studied under low magnification (X5). The autoradiographs will be compared with the microstructure and mineral phases of the wafer surfaces and correlations made between sorption and these parameters. Individual mineral phases exhibiting selective uptake will be used as sorptive substrates in future experiments.

Literature Cited

1. Izett, G. A., U. S. Geol. Surv. TEM-836-C 1960.

2. Lloyd, M. H. and Haire, R. G., "Studies on the Chemical and Colloidal Nature of Pu (IV) Polymer" the XXIV th International Union of Pure and Applied Chemistry Congress", Hamburg, Germany, September, 1973.

3. Private Communication from Gary Beall (Oak Ridge National Laboratory) at the WISAP Contractors Information meeting, Seattle, Oct. 1-5, 1978.

4. Rai, D. and Serne, R. J. , "Solid Phases and Solution Species of Different Elements in Geologic Environments", Pacific Northwest Laboratory Report - 2651, March 1978.

5. Apps, J. A., Lucas, J., Mathur, A. K., and Tsao, L., "Theoretical and Experimental Evaluation of Waste Transport in Selected Rocks: 1977 Annual Report of LBL Contract No. 4590IAK". Lawrence Berkeley Laboratory Report - 7022, p. 8, September 1977.

6. Baes, C. F. and Mesmer, R. E. "The Hydrolysis of Cations", p. 169, Wiley-Interscience Publications, N. Y., 1976.

7. Cleveland, J. M. "The Chemistry of Plutonium", p. 81, Gordon and Breach Science Publications, N. Y., 1970.

8. Sillen, L. G. and Martell, A. E., "Stability Constants of Metal Ion Complexes", Spec. Publ. No. 17, The Chemical Society, London, 1964.

9. Rai, D., Serne, R. J. and Swanson, J. L., "Solution Species of ^{239}Pu in Oxidizing Environments: II. Plutonyl (V)", Pacific Northwest Laboratory Report - 7027, June, 1978.

10. Smith, R. M. and Martell, A. E., "Critical Stability Constants", vol. 4: Inorganic Complexes, p. 37, Plenum Press, N. Y., 1976.

11. Allard, B. and Beall, G. W., "Predictions of Actinide Species in the Groundwater", Workshop on the Environmental Chemistry of the Actinide Elements, Warrington, Virginia, October 9, 1978.

Table I. Isotopic Abundances of Actinide Tracers

Element	Isotope	% by alpha activity	% by weight	Photon used for γ counting
Uranium	^{233}U	99.57	99.99+	Th L X-rays
	^{232}U	0.43	0.0002	
Neptunium	^{237}Np	100	100	86 and 29 kev γ-rays
Plutonium	^{242}Pu	84.08	99.91	
	^{240}Pu	4.58	0.091	
	^{238}Pu	11.32	0.003	
	^{237}Pu	0.02	~ 0.0002	Np K X-rays
Americium	^{243}Am	97.42	99.84	75 kev γ-rays
	^{241}Am	2.54	0.15	
Curium	^{248}Cm	1.86	95.76	
	^{246}Cm	5.45	3.87	
	^{244}Cm	0.51	0.0014	
	^{243}Cm	92.17	0.38	Pu K X-rays

TABLE II. X-ray Diffraction Data for Highly Altered Quartz Monzonite (U15E-7a)

METALLIC SAMPLE	DARK-GREY SAMPLE
Pyrite	Pyrite
Calcite	Calcite
Muscovite/Sericite	Muscovite/Sericite
Quartz	K-keldspar

YELLOW-GREY	PINK SAMPLE
Pyrite	Muscovite/Sericite
Calcite	K-feldspar
Muscovite/Sericite	Quartz
Quartz	
K-feldspar	
Clinozoisite	

TABLE II. X-ray Diffraction Data for Highly Altered Quartz Monzonite (U15E-7a)

METALLIC SAMPLE	DARK-GREY SAMPLE
Pyrite	Pyrite
Calcite	Calcite
Muscovite/Sericite	Muscovite/Sericite
Quartz	K-keldspar

YELLOW-GREY	PINK SAMPLE
Pyrite	Muscovite/Sericite
Calcite	K-feldspar
Muscovite/Sericite	Quartz
Quartz	
K-feldspar	
Clinozoisite	

TABLE III. Physical Property Data

	LAB	DC3-3600	DH5-2831	U15E-7	U15E-7a	UE-17E	DC3-3600 (powder)	U15E-7 (powder)	UE-17E (powder)
Recovery Depth (m)									
Hg Bulk Density (g/cc)	MM(2)	2.94	2.17	2.16	2.18	2.49	-	-	-
Hg Density at 50,000 psi (g/cc)	MM	3.43	2.60	2.38	2.39	2.68	-	-	-
Average Pore Diameter (μm)	MM	0.0044	0.0106	76	40	0.0104	-	-	-
Net Pore Volume (cc/g)	MM	0.016	0.057	0.42	0.041	0.019	-	-	-
Porosity, Hg Injection (%)	MM	14.3	16.7	9.2	8.8	7.1	-	-	-
Porosity, Gas Volume (%)	TT(3)	6.4	8.3	6.4	6.5	7.7	-	-	-
Specific Surface Area (ORR Analyzer) m^2/g)	MM	8.36	16.4	0.376	0.123	8.54	8.01	4.76	19.8
Specific Surface Area (Quantasure Analyzer) (m^2/g)	LBL(4)	4.57	-	-	-	6.44	-	-	-
Gas Permeability (Darcies)	TT	$7x10^{-3}$(1)	$3x10^{-4}$(1)	$<1x10^{-7}$	$<1x10^{-7}$	$<1x10^{-7}$	-	-	-

(1) Fracture permeability
(2) Analysis done by Micromeritics
(3) Analysis done by Terra Tek
(4) Analysis done by Lawrence Berkeley Laboratory Molecular Materials Research Division

TABLE IV. Tracer Purification and Oxidation State Selection

Method: Cation Exchange Column

HCl Elution

Dowex 50 x 8 Resin

0.5 cm diam x 12 cm long - 26°C

Elution Conc. HCl	Species
3 M	UO_2^{++}
0.5 M	NpO_2^{+}
9 M	Pu^{4+}
6 M	Am^{3+}
6 M	Cm^{3+}

TABLE V. Depth-of-Leaching Calculations

	BASALT (DC3-3600)	QUARTZ MONZONITE (U15E-7)
total moles per gram of sample	.0411	.0473
unit cell edge (A)	2.28	2.45
most mobile ion	Na	Mg
mobile ion mole fraction	.0249	.00535
surface sites in 120 g sample	1.85×10^{22}	1.61×10^{22}
layers leached (846 hr)	5.9	11
leach depth (A) (846 hr)	13	26
linear region leach rate (layers hr^{-1})	0.35×10^{3}	1.75×10^{-3}

TABLE VI. Comparison of Prepared Waters With Waters From Natural Systems (mg/1)

	DC3-3600	(1)	U15E-7	(2)	(3)	UE-17E	(4)	(5)
Na	52	37	20	93	6.0	77	12	18
K	8.0	7.0	26	3.0	1.6	9.0	1.1	1.5
Mg	4.4	8.0	19	18	1.7	13	16	19
Ca	11	19	38	117	10	32	29	96
Fe	1.2	0.2	2.3	0.2	.01	1.4	.02	1.0
Al	.12	-	.01	0.2	.02	.01	0	0
SiO_2	63	55	42	33	25	33	16	15
pH	6.4	7.8	6.6	7.6	6.8	6.8	4.9	7.8
HCO_3	190	150	290	214	57	380	126	133
Cl	1.5	10	1.5	32	1.1	0.8	12	25
SO_4	2	20	2	337	2.4	3	22	208

(1) Average composition of groundwaters from Columbia River basalts (525 samples).
(2) Seepage waters from climax stock (quartz monzonite).
(3) Average composition of perennial springs in quartz monzonites and granodiorites of the Sierra Nevadas (56 samples).
(4) Groundwater from the Brunswick Shale of New Jersey.
(5) Groundwater from the Chicopee Shale of Massachusetts.

TABLE VII. Adsorption Coefficients, $K = \frac{d/m/gm}{d/m/ml}$

I = Basalt, II = Shale, III = Quartz monzonite, A = Altered

Sample	$\frac{Up}{Down}$	K(alpha)	K(filter)	K(gamma)
I - U	1.51	1.87	2.01	2.80
II - U	7.78	0.761	0.797	6.65
III - U	2.33	0.316	0.343	0.287
I - Np	1.09	0.416	0.394	0.459
II - Np	0.797	1.53	1.29	48.7
III - Np	1.53	0.199	0.204	0.471
I - Pu	4.33	48.9	423	60.1
I - Pu - A	7.00	137		139
II - Pu	3.50	188	729	145
III - Pu	7.37	261	2973	225
III - Pu - A	11.0	113		143
I - Am	7.73	1270	14300	1033
II - Am	3.02	97.8	394	962
III - Am	6.02	1290	12700	1323
I - Cm	4.35	746	4900	525
II - Cm	2.78	44.2	724	219
III - Cm	3.29	164	6460	171

TABLE VIII. Desorption Coefficients, $K = \frac{d/m/gm}{d/m/ml}$

I= Basalt, II= Shale, III= Quartz monzonite, A= Altered

Sample	$\frac{Up}{Down}$	K(alpha)	K(filter)
I - U	3.65	2.57	3.50
II - U	3.83	1,04	1.10
III - U	2.52	2.26	1.82
I - Np	1.35	1.45	1.19
II - Np	1.20	0.675	0.570
III - Np	1.10	3.86	2.90
I - Pu	5.20	67.3	777
I - Pu - A	2.18	345	
II - Pu	1.32	201	122
III - Pu	2.98	108	103
III - Pu - A	11.07	779	
I - Am	4.33	274	5331
II - Am	1.01	480	798
III - Am	4.71	186	1664
I - Cm	5.57	850	12672
II - Cm	1.75	187	1118
III - Cm	4.08	561	2676

Figure Captions

Fig. 1 Core processing (scale in cm). Samples taken for area, and pore size distribution measurements (A), petrographic thin sections (B_1, B_2 and B_3), sorption experiments (C_1 and C_2) and permeability measurements (D).

Fig. 2 Sodium released to the aqueous solution during the dissolution of powders from three rock types.

Fig. 3 Potassium released to the aqueous solution during the dissolution of powders from three rock types.

Fig. 4 Calcium released to the aqueous solution during the dissolution of powders from three rock types.

Fig. 5 Magnesium released to the aqueous solution during the dissolution of powders from three rock types.

Fig. 6 Aqueous silica released to the aqueous solution during the dissolution of powders from three rock types.

Fig. 7 Changes of pH during the dissolution experiments. Note the rapid initial decrease in the hydrogen ion concentration.

Fig. 8 Percentage of initial concentrations of tracers left in solution as a function of time for the sorption experiments with the blank containers.

Fig. 9 Percentage of initial concentrations of tracers left in solution as a function of time for the sorption experiments with the basalt samples.

Fig. 10 Percentage of initial concentrations of tracers left in solution as a function of time for the sorption experiments with the shale samples.

Fig. 11 Percentage of initial concentrations of tracers left in solution as function of time for the sorption experiments with the quartz monzonite samples.

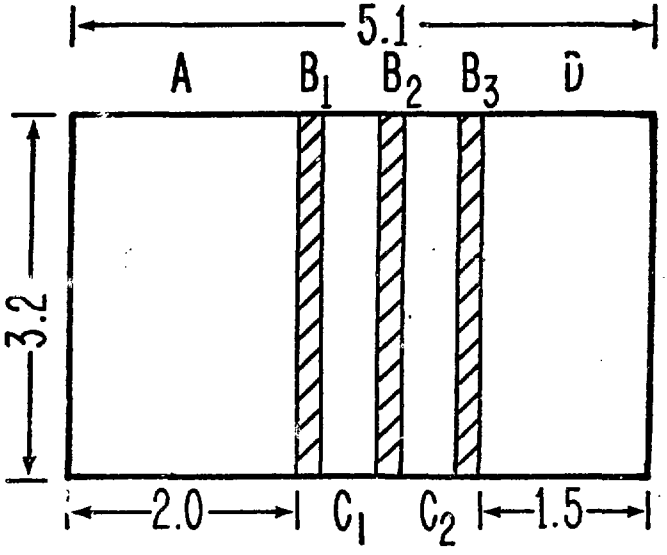

XBL 788-2043

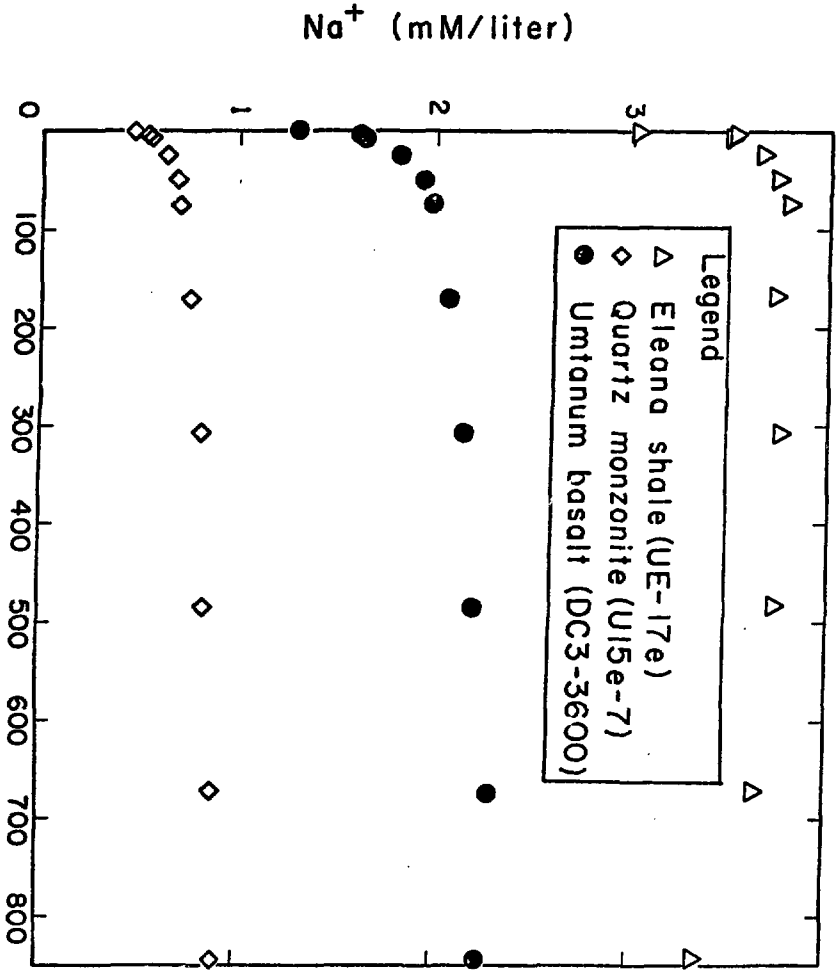
Na+ (mM/liter)
0
1
2
3
0
100
200
300
400
500
600
700
800
time (hrs).
Legend
Eleana shale (UE-17e)
Quartz monzonite (U15e-7)
Umtanum basalt (DC3-3600)

XBL787-2044

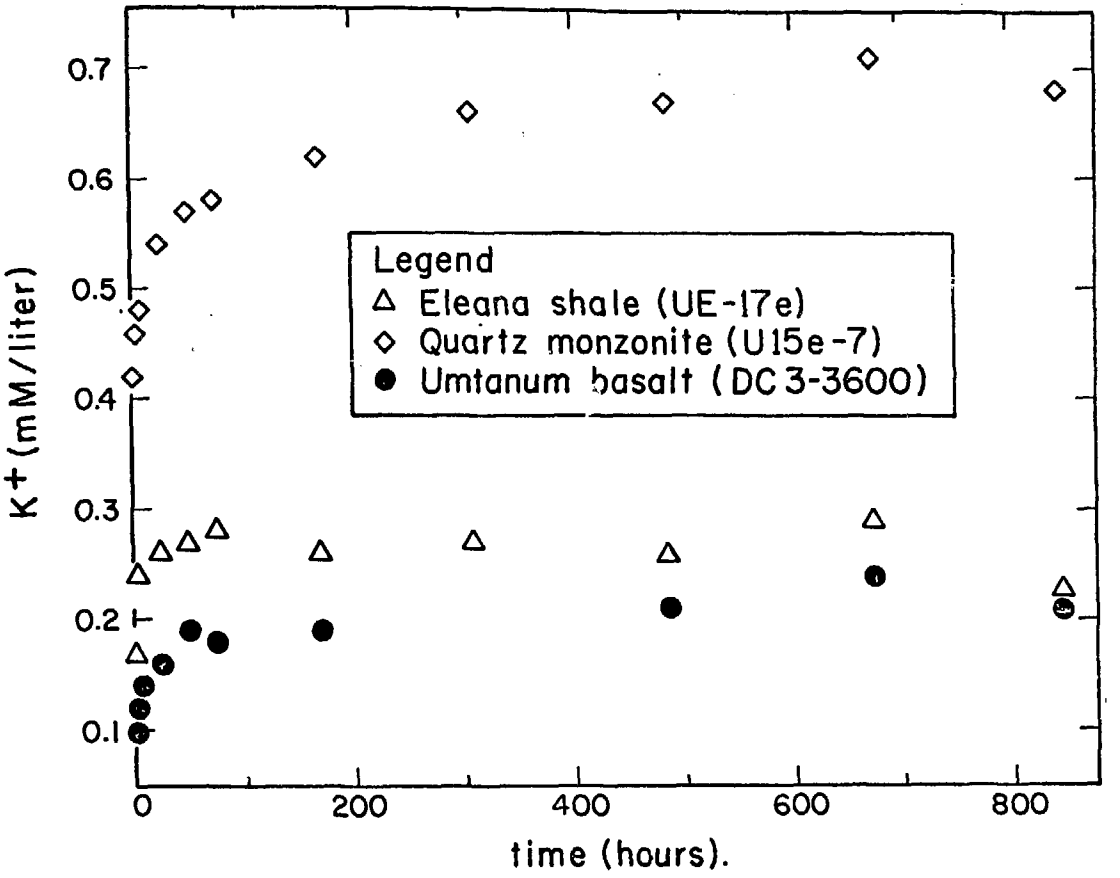
0.7
0.6
0.5
0.4
0.3
0.2
0.1
K+ (mM/liter)
0
200
400
600
800
time (hours).
Legend
Eleana shale (UE-17e)
Quartz monzonite (U15e-7)
Umtanum basalt (DC 3-3600)

XBL 788-2046

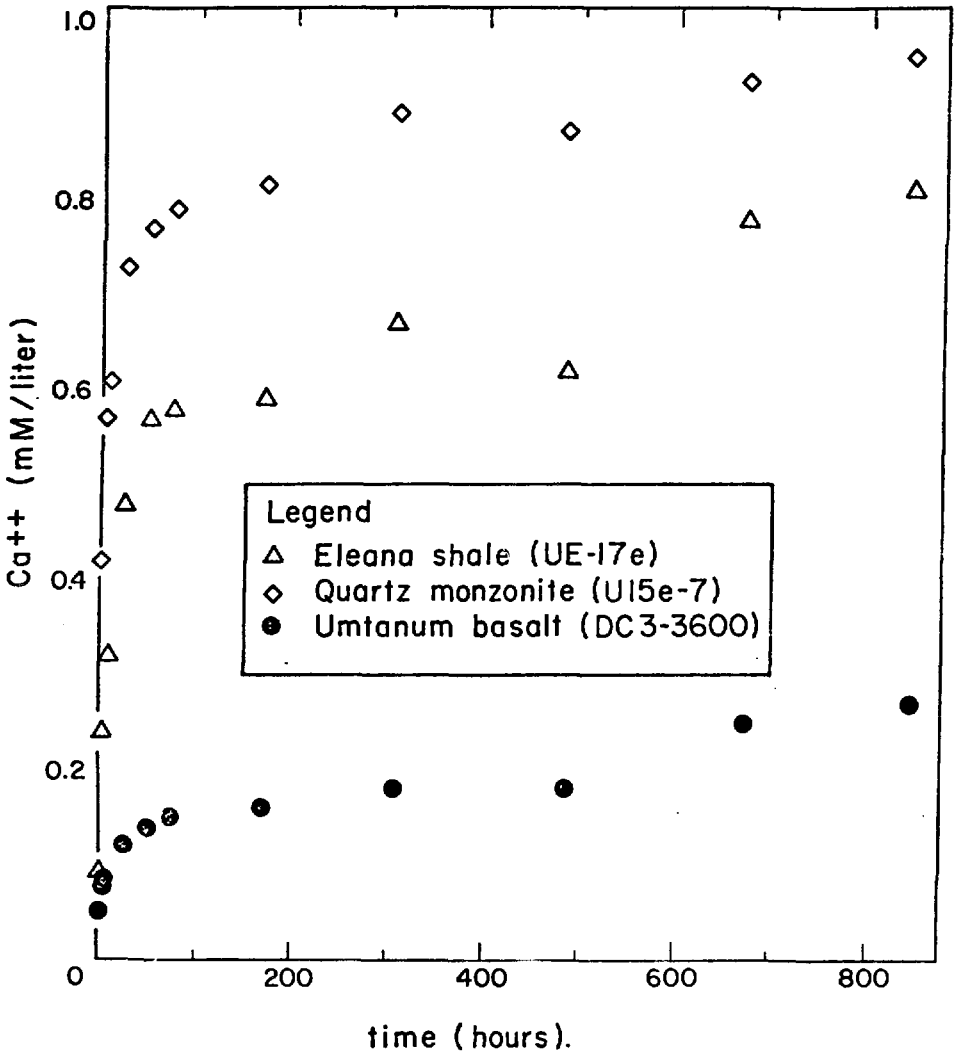
1.0
0.8
0.6
0.4
0.2
0
Ca++ (mM/liter)
200
400
600
800
time (hours).
Legend
Eleana shale (UE-17e)
Quartz monzonite (U15e-7)
Umtanum basalt (DC3-3600)

XBL 788-2049

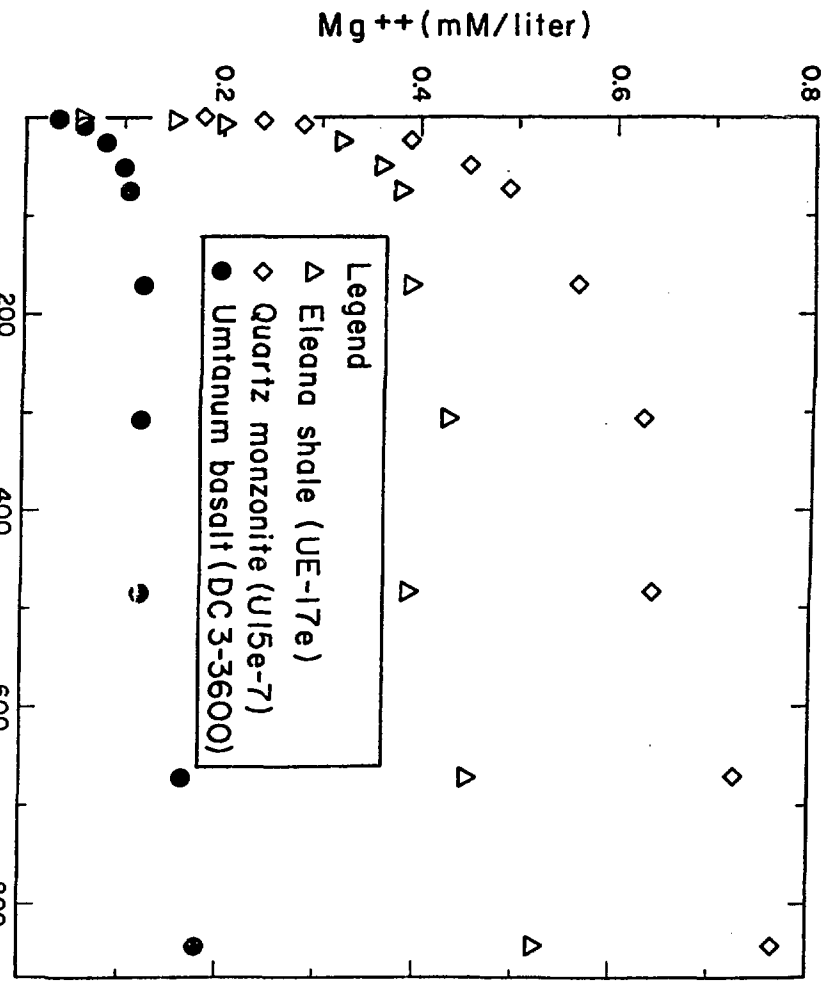
Mg ++ (mM/liter)
0.2
0.4
0.6
0.8
200
400
600
800
time (hours).
Legend
Eleana shale (UE-17e)
Quartz monzonite (U15e-7)
Umtanum basalt (DC 3-3600)

XBL 788-2048

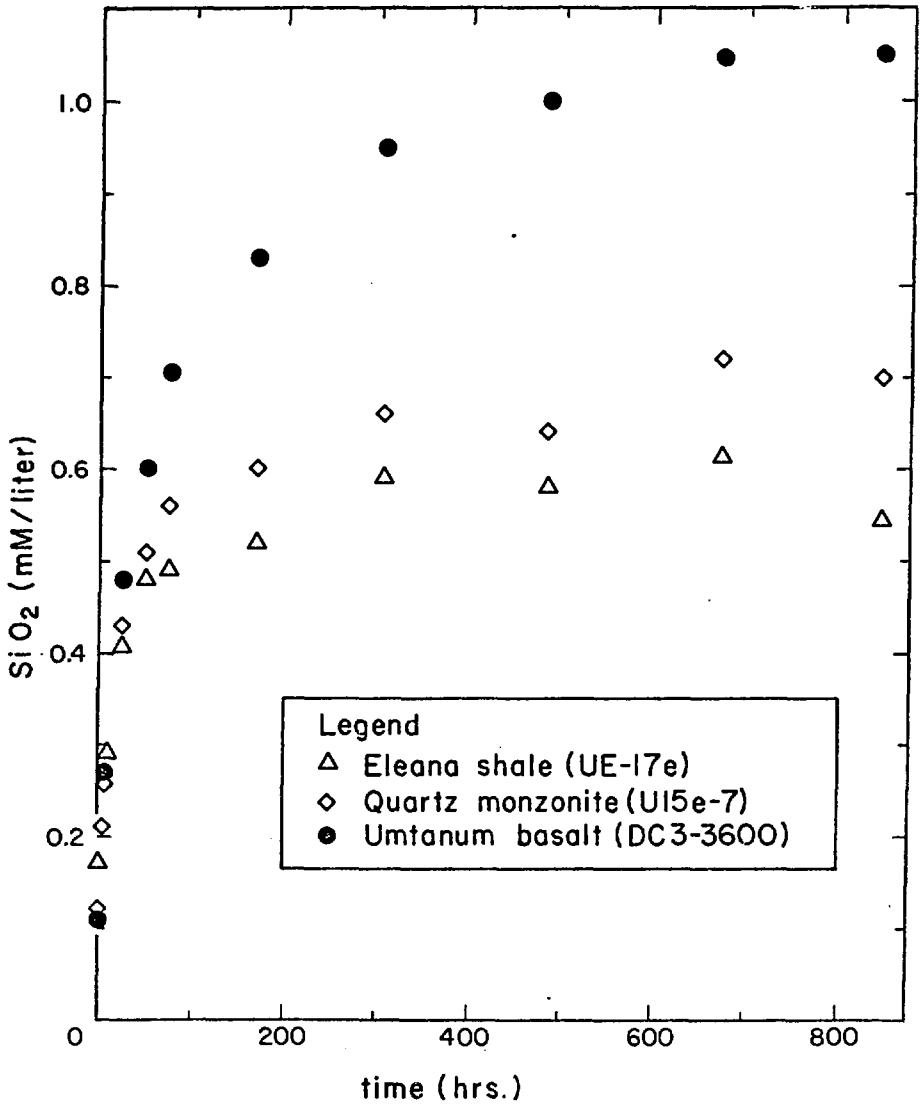
1.0
0.8
0.6
0.4
0.2
0
Si O2 (mM/liter)
200
400
600
800
time (hrs.)
Legend
Eleana shale (UE-17e)
Quartz monzonite (U15e-7)
Umtanum basalt (DC3-3600)

XBL 788-2047

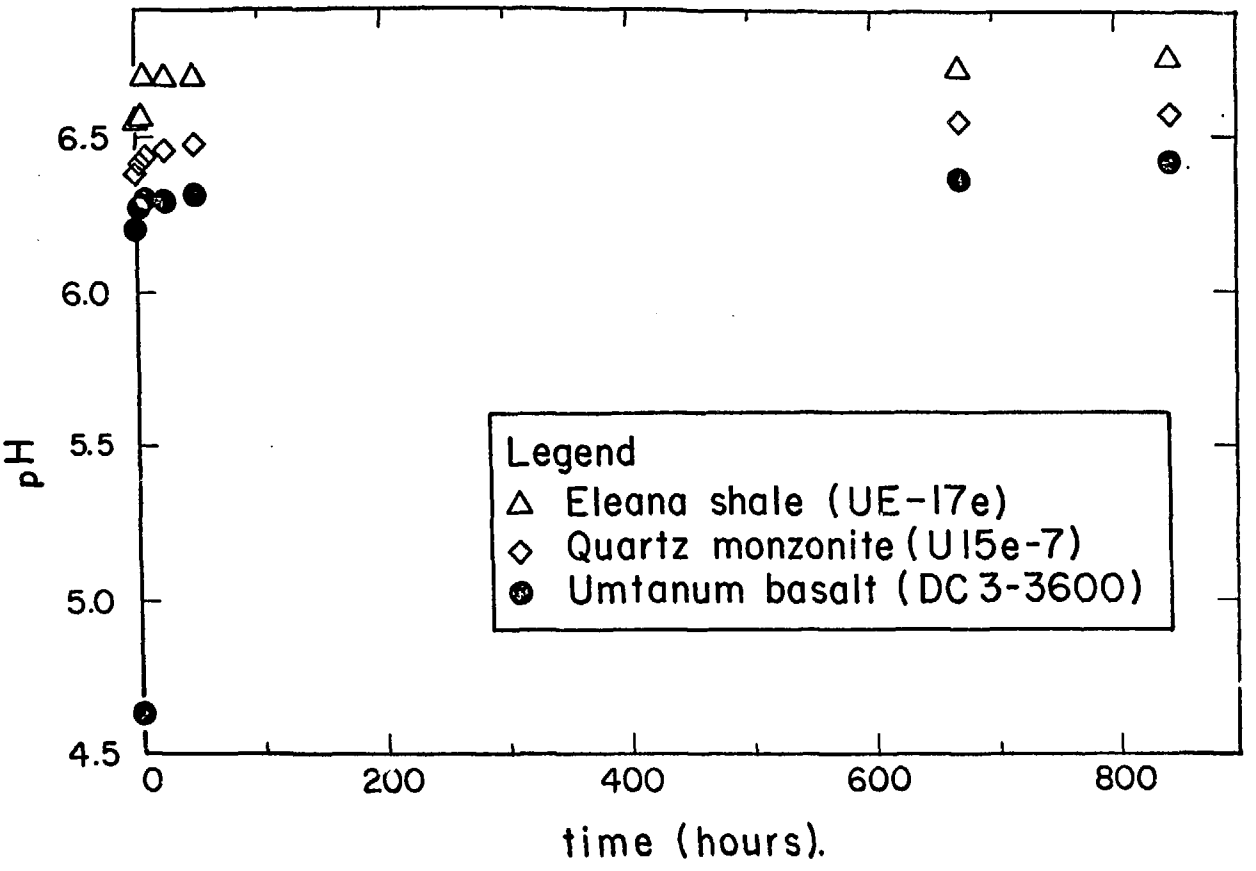
pH
6.5
6.0
5.5
5.0
4.5
0
200
400
600
800
time (hours).
Legend
Eleana shale (UE-17e)
Quartz monzonite (U15e-7)
Umtanum basalt (DC 3-3600)

XBL 788-2045

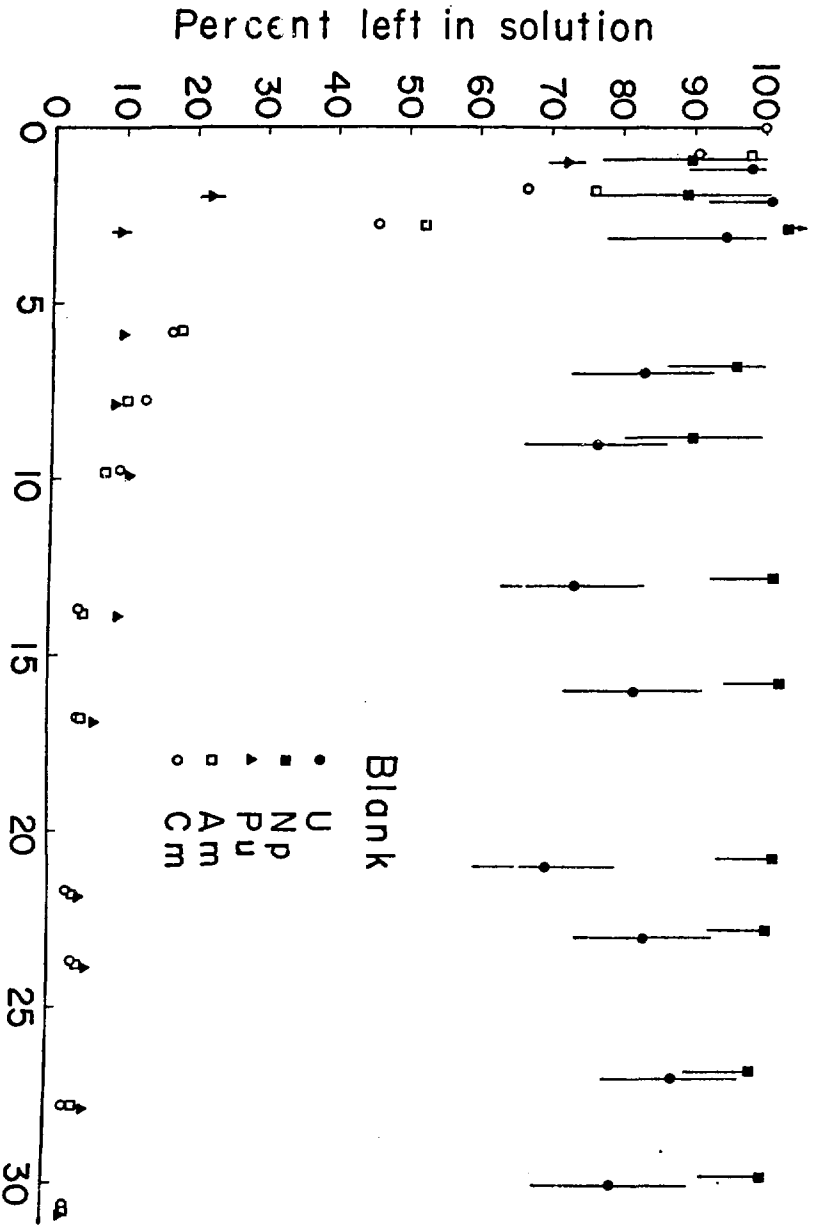
Percent left in solution
0
10
20
30
40
50
60
70
80
90
100%
0
5
10
15
20
25
30
Time (days)
Blank
U
Np
Pu
Am
Cm

XBL 786-1883

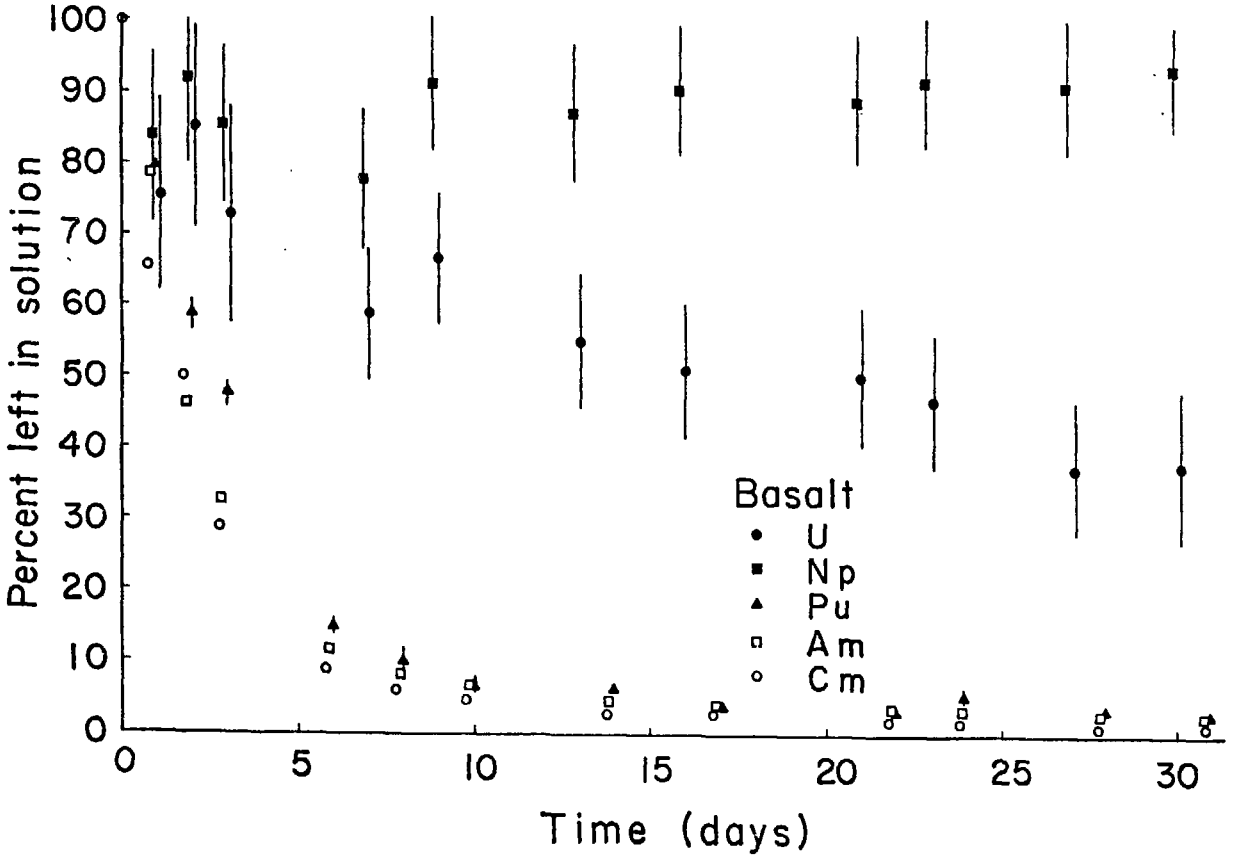
Percent left in solution
Time (days)
Basalt
U
Np
Pu
Am
Cm
0
10
20
30
40
50
60
70
80
90
100
0
5
10
15
20
25
30

XBL 786-1882

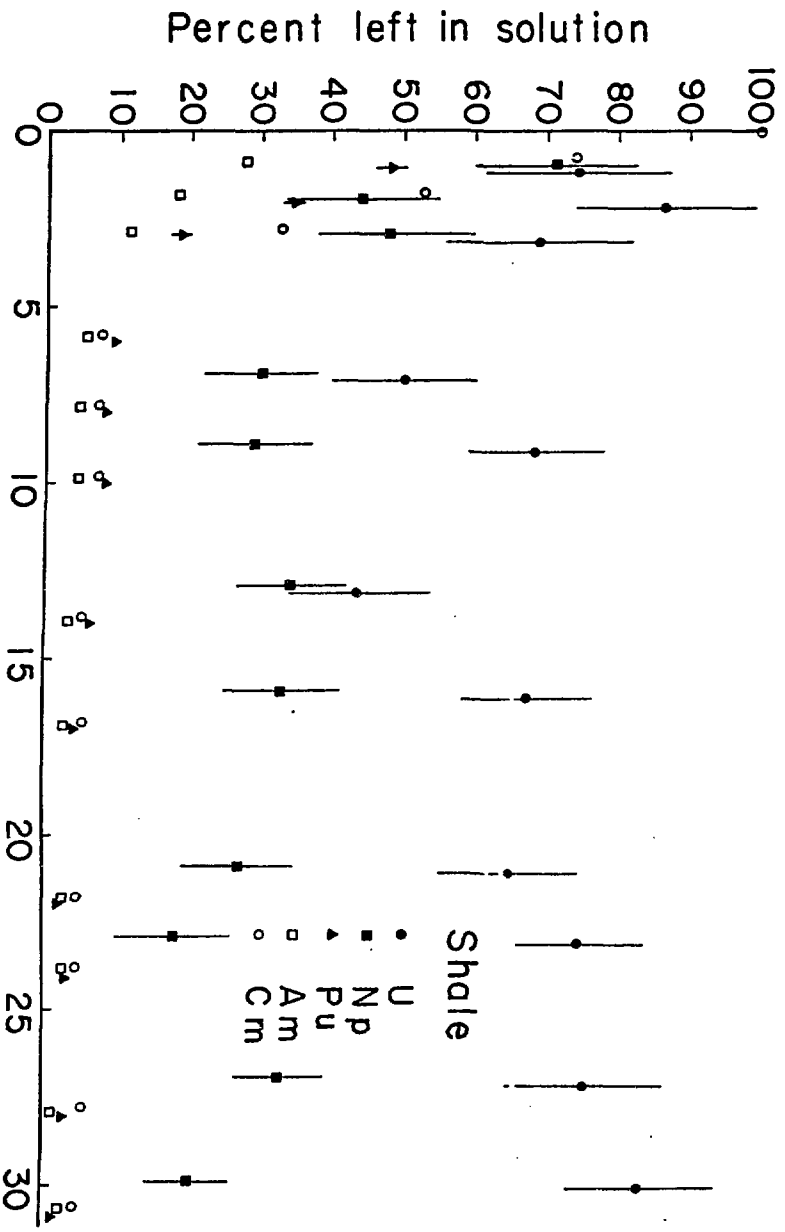
Percent left in solution
0
10
20
30
40
50
60
70
80
90
100
Time (days)
0
5
10
15
20
25
30
Shale
U
Np
Pu
Am
Cm

XBL 786-1884

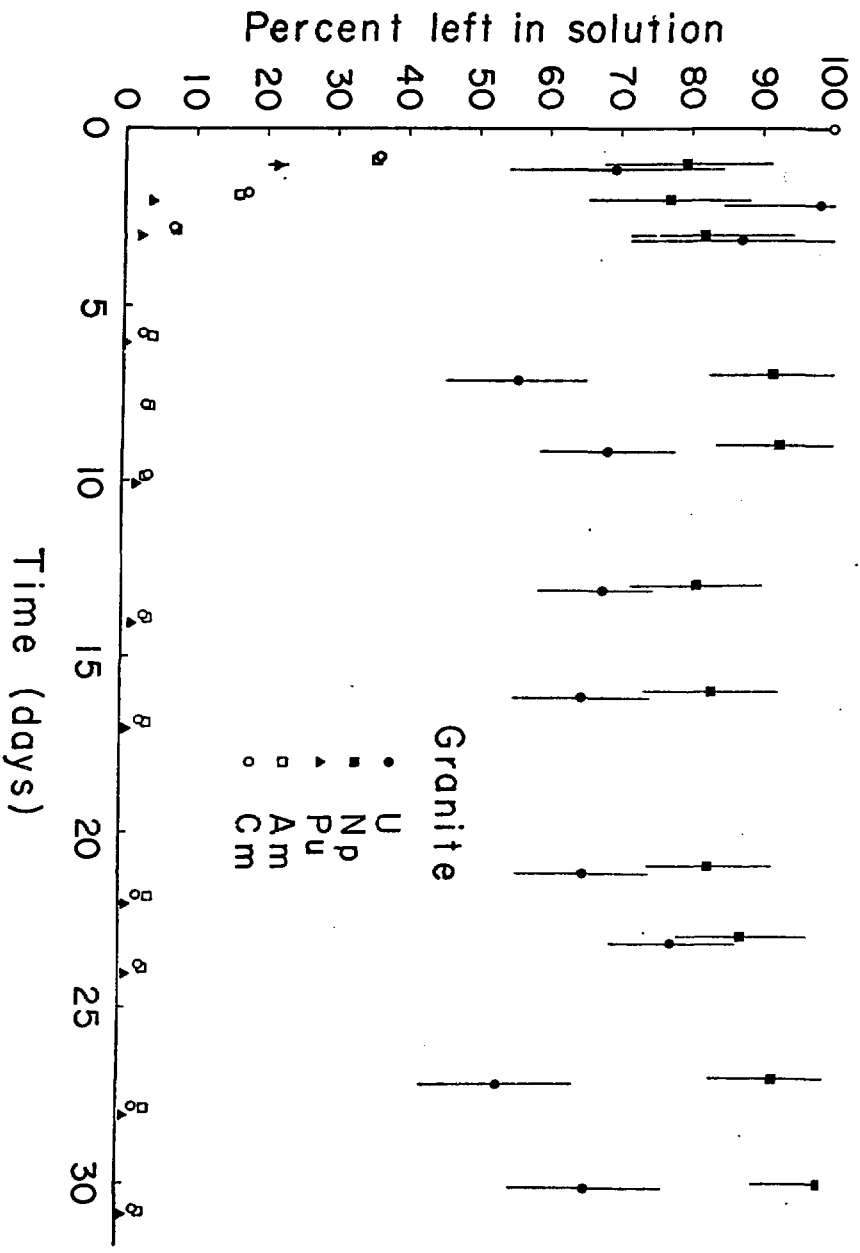
Percent left in solution
0
10
20
30
40
50
60
70
80
90
100
0
5
10
15
20
25
30
Time (days)
Granite
U
Np
Pu
Am
Cm

XBL 786-1881